Biosensors and Bioelectronics 56 (2014) 313–319

Contents lists available at ScienceDirect

Biosensors and Bioelectronics

journal homepage: www.elsevier.com/locate/bios

Shape-dependent electron transfer kinetics and catalytic activity of NiO nanoparticles immobilized onto DNA modified electrode: Fabrication of highly sensitive enzymeless glucose sensor

Ensiyeh Sharifi [a], Abdollah Salimi [b,c,*], Esmaeil Shams [a,**], Abdollah Noorbakhsh [d], Mohammad K. Amini [a]

[a] Chemistry Department, University of Isfahan, Hezar Jarib, Isfahan 81746-73441, Iran
[b] Department of Chemistry, University of Kurdistan, P.O. Box 416, Sanandaj, Iran
[c] Research Center for Nanotechnology, University of Kurdistan, P.O. Box 416, Sanandaj, Iran
[d] Department of Nanotechnology Engineering, Faculty of Advanced Science and Technology, University of Isfahan, Hezar Jarib, Isfahan 81746-73441, Iran

ARTICLE INFO

Article history:
Received 5 November 2013
Received in revised form
30 December 2013
Accepted 3 January 2014
Available online 14 January 2014

Keywords:
Nickel oxide
Triangular nanoparticles
DNA
Glucose
Enzymeless biosensor

ABSTRACT

Herein we describe improved electron transfer properties and catalytic activity of nickel oxide nanoparticles (NiONPs) via the electrochemical deposition on DNA modified glassy carbon electrode (DNA/GCE) surface. NiONPs deposited on the bare and DNA-coated GCE showed different morphologies, electrochemical kinetics and catalytic activities. The atomic force microscopy (AFM) images revealed the formation of triangular NPs on the DNA/GCE that followed the shape produced by the DNA template, while the electrodeposition of NiONPs on the bare GCE surface led to the formation of spherical nanoparticles. Electrochemical impedance spectroscopy (EIS) measurements revealed lower charge-transfer resistance (R_{ct}) of triangular NiONPs compared to spherical NPs. Furthermore, the electrocatalytic activity of triangular NiONPs compared to spherical NPs toward glucose oxidation in alkaline media was significantly improved. The amperometric oxidation of glucose at NiONP–DNA/GCE, yielded a very high sensitivity of 17.32 mA mM^{-1} cm^{-2} and an unprecedented detection limit of 17 nM. The enhanced electron transfer properties and electrocatalytic activity of NiONP–DNA/GCE can be attributed to the higher fraction of sharp corners and edges present in the triangular NiONPs compared to the spherical NPs. The developed sensor was successfully applied to the determination of glucose in serum samples.

© 2014 Elsevier B.V. All rights reserved.

1. Introduction

Nickel oxide (NiO) is one of the most important transition metal oxides and has received considerable interests due to its useful electronic and electrochemical properties (Thimsen et al., 2012). NiO nanoparticles (NiONPs) exhibit electronic, catalytic and magnetic properties that are different from those of the bulk material (Peck and Langell, 2012; Welch and Compton, 2006). The catalytic ability of NiONPs make them attractive for applications in various fields of technology, such as batteries and fuel cells (Wu and Chang, 2013), chemical synthesis (Khairy et al., 2012), and electrochemical-based sensors (Sharifi et al., 2013). Different electrochemical sensors based on the electrocatalytic activity of NiONPs have been developed for the determination of various biological compounds such as H_2O_2 (Yin et al., 2011), glucose (Niu et al., 2013), methanol (Jiang et al., 2010), amoxicillin (Ojani et al., 2012), and insulin (Salimi et al., 2007a). Recently, the electrocatalytic activity of Ni-based sensors toward glucose oxidation has been greatly increased (Gao et al., 2011; Niu et al., 2013; Wang et al., 2010) due to their ease of performance, low cost and high sensitivity.

Among the various methods that have been developed for the preparation of NiONPs, the in-situ electrochemical deposition of particles on the electrode support is a fast and simple technique that provides an effective tool for controlling the size and morphology of NiONPs (Salimi et al., 2007b). It is now well-known that the chemical and physical properties of NPs as well as their catalytic activity depend on the size, shape, and composition of particles (Sun and Xia, 2002). The kinetic parameters of NPs are believed to be correlated to the calculated fraction of surface atoms located on the corners and edges in each size and shape (Narayanan and El-Sayed, 2004a). The effect of nanoparticles size and shape on their catalytic activity has been reported (Narayanan and El-Sayed, 2004b; Xu et al., 2006). Different methods for the

* Corresponding author at: Department of Chemistry, University of Kurdistan, 66177-15175, Sanandaj, Iran. Tel.: +98 8716624001; fax: +98 8716624008.
** Corresponding author: Tel: +98 311 7932708; fax: +98 311 6689732.
E-mail addresses: absalimi@uok.ac.ir (A. Salimi), e_shams@chem.ui.ac.ir (E. Shams).

0956-5663/$ - see front matter © 2014 Elsevier B.V. All rights reserved.
http://dx.doi.org/10.1016/j.bios.2014.01.010

manufacture of 2D and 3D NPs structures on surfaces have been developed (Gao et al., 2011; Niu et al., 2013). Biomaterials assembled on suitable surfaces can provide templates for the immobilization of NPs which lead to the fabrication of novel NP–biomolecule hybrid systems (Lakowicz et al., 2000). Single or double-stranded DNA molecules, which are fixed at a surface of a solid support, have been used as a template for the generation of nanostructures. Kumar et al. (2001) indicated that the deposition of positively charged lysine-capped AuNPs on a surface that was covered with a thick layer of negatively charged DNA film led to the assembly of nanoparticles into linear superstructures that followed the shape of the DNA template. In addition, the unique three-dimensional structure of DNA has been reported to lead a 500-fold enhancement in its specific surface area (Lin et al., 2005). So, the immobilization of DNA molecules on the electrode surface can supply more sites for the immobilization of NPs. Nowadays, NPs–DNA composites have a promising application in a number of novel technologies including molecular diagnosis, gene therapy and sensing (An and Jin, 2012). The integration of NiONPs, which show unique catalytic, electronic and magnetic properties, with DNA, which displays unique three dimensional structures, can yield a very promising NiONP–DNA nanocomposite with new functionalities in the development of biosensors and bioelectronic devices. In the present study we report immobilization of a stable film of calf thymus (CT) ds-DNA on GCE surface and its implementation as a support for electrochemical deposition of NiONPs. We demonstrate that the DNA film provides an improved surface for electrodeposition of NiONPs and acts as a template for the formation of triangular nanoparticles, resulting in a remarkable enhancement of the electrocatalytic activity of the electrode. As a proof of improved electrocatalytic activity, the modified electrode (NiONP–DNA/GCE) was used to investigate the oxidation of glucose in alkaline media. The application of the proposed modified electrode toward nanomolar detection of glucose was evaluated using hydrodynamic amperometry technique.

2. Experimental

The details of experiments are given in Supporting information (SI). Briefly, the GCE was immersed in a solution containing 1 mg ml^{-1} DNA and the potential was repetitively cycled (40 scans) from 1.5 to 1.7 V at a scan rate of 100 mV s^{-1} (Lin et al., 2005). This electrode was thoroughly washed with distilled water to remove any unadsorbed or weakly-adsorbed DNA and denoted as DNA/GCE. Further modification was performed by depositing metallic nickel in situ on the DNA/GCE under a constant potential of −0.8 V for 10 s in acetate buffer solution (pH 6) containing 1 mM nickel nitrate. Then, the electrode was washed with water and immersed into a 0.1 M NaOH solution and cyclic scans were performed in the potential range of 0.0–0.6 V (30 scans) at a scan rate of 100 mV s^{-1} for the electrodissolution of Ni and formation of a passive NiO layer on the DNA/GCE surface (Giovanelli et al., 2003). The obtained electrode was described as NiONP–DNA/GCE. The NiONP/GCE was prepared under the same procedure in the absence of DNA.

3. Results and discussion

3.1. Surface characterization of modified electrodes

The surface morphology of the GCE during modification by DNA and NiONPs was characterized by AFM. The corresponding AFM measurements indicated that the NiONPs immobilized on the DNA/GCE are obviously different in their shapes and sizes from those directly deposited on the GCE surface. The AFM images of the NiONP/GCE (Fig. 1A and C) indicates the formation of spherical nanoparticles with an average diameter of 600 nm, while, for NiONP–DNA/GCE (Fig. 1B and D), triangular nanoparticles with an average height of 50 nm and in-plane width of 500 nm uniformly distributed over the DNA/GCE surface (Fig. S1). When DNA templates are fixed at a surface of a solid support, the resulting assemblies of NPs may be expected to have a pattern that is dependent on the pattern produced upon the DNA immobilization. The AFM images revealed that the clean bare GCE has a flat surface, which was different from that of the DNA/GCE surface (Fig. S2A and B). As can be seen the DNA layer is formed in nearly similar pattern to the NiONP–DNA nanostructure, and it can be concluded that DNA molecules acted as a template for growing of triangular NiONPs.

3.2. Electrochemical characterization: voltammetric study

The cyclic voltammogram (CV) of the DNA/GCE was recorded in pH 7.0 (PBS). A small irreversible voltammetric wave found around +0.9 V is attributed to the oxidation of guanine bases of DNA molecules (see Fig. S3), confirming the successful immobilization of DNA on the GCE surface. The electrochemical activity of the electrodeposited NiONPs was investigated by recording CVs of the modified electrodes in 0.5 mM NaOH solution. Fig. 1E shows the CVs of NiONPs deposited on the bare GCE (NiONP/GCE, curve a) and DNA modified GCE (NiONP–DNA/GCE, curve b), produced under the same conditions (10 s deposition at a constant potential of −0.8 V from the same solutions). The anodic peak observed at 0.38 V is attributed to the oxidation of the β-Ni(OH)$_2$ phase to β-NiOOH, and the corresponding cathodic peak at 0.32 V represents reduction of β-NiOOH to Ni(OH)$_2$ (Giovanelli et al., 2003). During positive voltage scan, α-Ni(OH)$_2$ and β-Ni(OH)$_2$ phases are oxidized and converted to β-NiOOH and γ-NiOOH phases. Due to formation of passive film of β-Ni(OH)$_2$ on the electrode surface during negative potential scan, the β-NiOOH is not fully reduced to its starting material and the high reduction peak current compared to oxidation peak current is decreased (Zhang and Park, 1998).

It is clear that in the presence of DNA, there is a large increase in the peak current of NiONP (by an order of magnitude) compared with the current obtained in the absence of DNA. The amount of the electrodeposited NiONPs on the electrode surface can be estimated as an effective surface concentration, Γ (Sharifi et al., 2013):

$$\Gamma = Q_{OX}/nFA \quad (1)$$

where F is the Faraday number, n is the number of electrons involved in the redox process ($n=1$), Q_{ox} is the charge associated with the oxidation of Ni(OH)$_2$, and A is the geometric surface area of the electrode (0.0314 cm^{-2} for GCE and 0.0381 for DNA/GCE). According to Eq. (1), Γ values were calculated to be 6.2 and 39.2 nmol cm^{-2} for NiONP/GCE and NiONP–DNA/GCE, respectively, indicating a remarkable increase in the amount of NiONPs deposited on the surface of the electrode modified with DNA molecules. This behavior can be the result of two effects: (i) the immobilization of DNA may form a network on the GCE surface which increases the overall surface area of the electrode; we expected that NiONPs should deposit on the DNA chains and not directly on the GCE surface, resulting in a significant increase in the amount of the NiONPs electrodeposited on the surface and (ii) electrostatic attraction between the negatively charged DNA layer and Ni^{2+} ions, leading to deposition of more NiONPs on the surface. Since the surface area of the electrode increase a little with immobilization of DNA, the observed increase in the amount of NiONPs deposited on the surface is predominantly attributed to the effect of the electrostatic attraction between the negatively charged DNA layer and Ni^{2+} ions. The long term stability of NiONP–DNA/GCE was also studied and details are reported in the supplementary information.

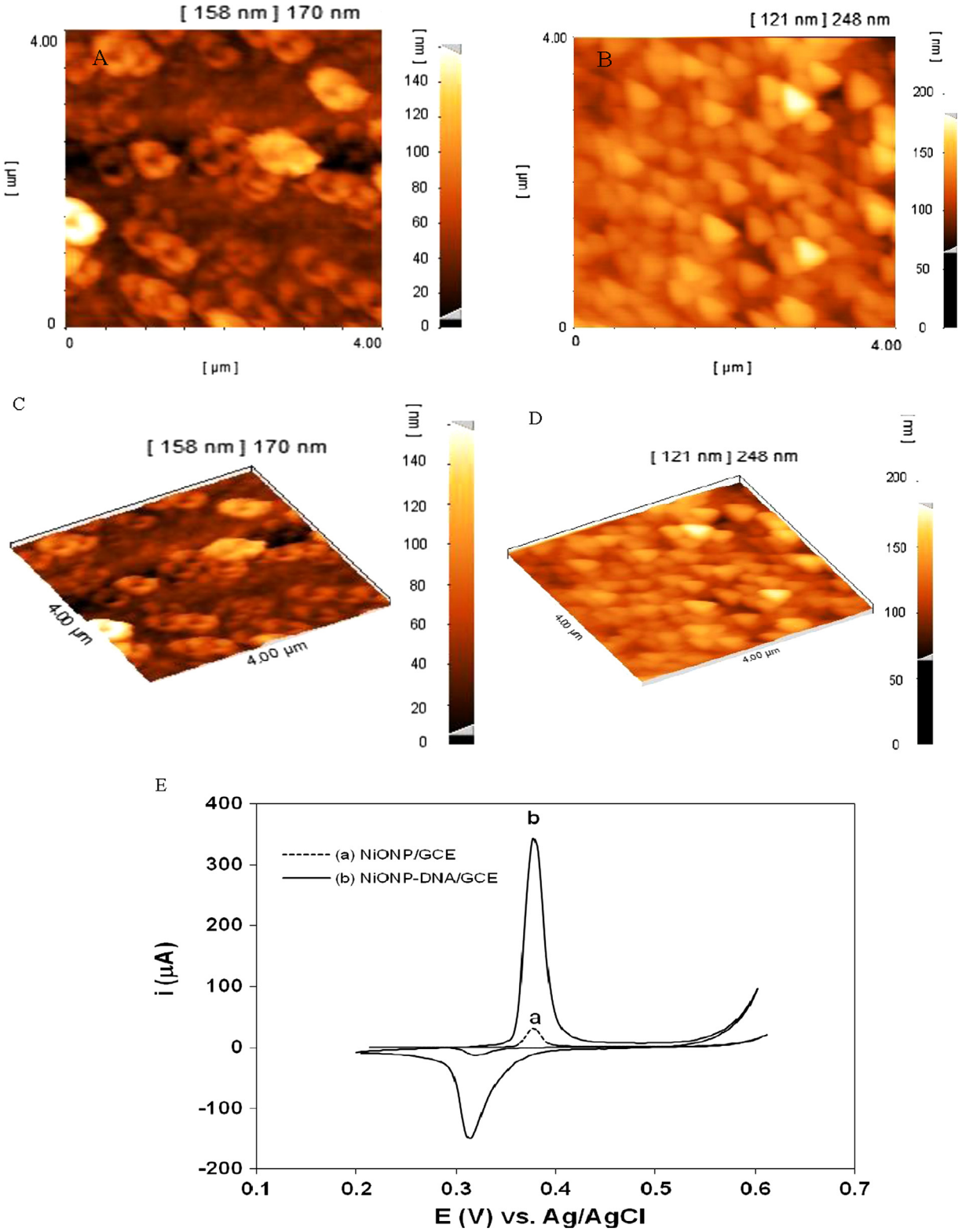

Fig. 1. AFM images of (A) NiONP/GCE and (B) NiONP–DNA/GCE; (C) and (D) 3D images of (A) and (B) respectively. (E) Recorded CVs of NiONP/GCE (a) and NiONP–DNA/GCE (b), in 0.5 M NaOH solution. Scan rate: 100 mV s^{-1}.

3.3. *Electrochemical impedance spectroscopy study*

Electrochemical impedance spectroscopy is a useful technique for characterization of modified electrodes (Noorbakhash and Salimi, 2011; Saadati et al., 2012; Karimi-Maleh et al., 2013; Elyasi et al., 2013). The stepwise modification of the GCE surface by DNA and NiONPs was probed in the presence of two external redox probes, $[Fe(CN)_6]^{3-/4-}$ and ferrocenemethanol (FcMeOH) (as ionic and natural probes, respectively), and the results are described in the following sections.

3.3.1. EIS study in the presence of $[Fe(CN)_6]^{3-/4-}$

Fig. 2A (a–d) shows EIS complex-plane plots, obtained at a potential of 0.22 V in 0.20 M KCl solution containing 0.5 mM $K_3[Fe(CN)_6]/K_4[Fe(CN)_6]$ (1:1), for bare GCE (a), NiONP/GCE (b), DNA/GCE (c) and NiONP–DNA/GCE (d). The charge transfer resistance (R_{ct}) is a key parameter for the kinetics of a probe at the electrode interface and it can be obtained by appropriate fitting of the impedance data to an appropriate model. The EIS data obtained on the modified electrodes in the presence of $[Fe(CN)_6]^{3-/4-}$ redox probe were approximated by using the modified Randles model (the inset of Fig. 2A) and the results are reported in Table 1A. The R_{ct} value increased from 423 Ω for the bare GCE (curve a) to about 21939 Ω for DNA/GCE (curve c). This behavior can be related to (i) impeding electron transfer at the electrode surface by DNA backbone, and (ii) electrostatic repulsion between negatively charged DNA/GCE surface and $[Fe(CN)_6]^{3-/4-}$ probe. The results confirm successful immobilization of DNA onto the GCE surface, although the predominant effect is not clearly known. The R_{ct} value decreased to 1069 Ω upon deposition of NiONPs on the DNA layer (curve d), showing that the assembly containing NiONPs facilitates electron transfer of the redox probe. In an attempt to find out possible mechanisms for the formation of NiONPs on the GCE surface in the presence and absence of DNA strands, we compared the EIS data obtained for NiONP/GCE and NiONP–DNA/GCE. Interestingly, the results exhibit that R_{ct} for NiONP/GCE (curve b) is 6993 Ω, much higher than that for the NiONP–DNA/GCE (curve d, $R_{ct} \cong 1069$ Ω), under the same conditions. The experimental results, being a bit surprising, clearly indicate faster electron transfer at the NiONP–DNA/GCE interface compared to that of NiONP/GCE. Similar behavior was observed from CVs on the modified electrodes in the presence of $[Fe(CN)_6]^{3-/4-}$ couple (Fig. 2B), confirming the EIS results (R_{ct} is proportional to ΔEp and 1/Ip).

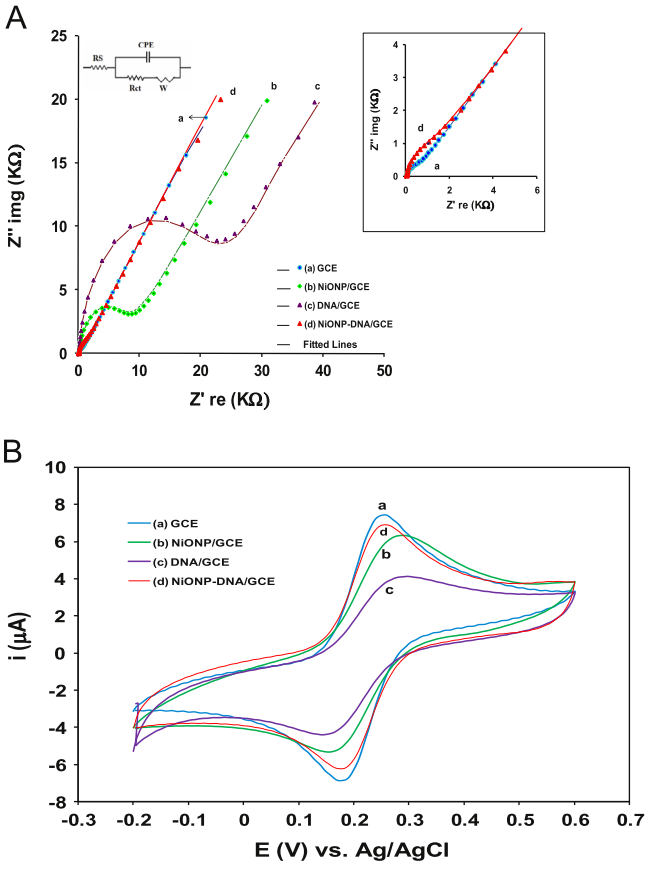

Fig. 2. (A) Nyquist plots and (B) CVs obtained on GCE (a), NiONP/GCE (b), DNA/GCE (c), and NiONP–DNA/GCE (d) in 0.2 M KCl solution containing 0.5 mM $K_3Fe(CN)_6+K_4Fe(CN)_6$. Scan rate: 100 mV s^{-1}. The EIS Nyquist plots obtained at an applied potential of 0.22 V and a frequency range of 0.01–1 × 10^4 Hz. Symbols and trend lines show the experimental and the fitted data based on modified Randle's model, respectively. Insets top right and left of figure (A) show the EIS Nyquist plots at high frequency range and Equivalent circuit model used for fitting the impedance data, respectively.

Table 1A
Electrochemical parameters extracted from EIS data (Fig. 2) obtained on different modified electrodes in 0.2 M KCl containing 0.5 mM $[Fe(CN)_6]^{3-/4-}$.

Electrode	R_s (Ω)	R_{ct} (Ω)	n	K_{app} (cm s^{-1}) × 10^3
GC	75.3 ± 0.4	423 ± 6	0.913 ± 0.004	40 ± 0.9
NiONP/GC	100.7 ± 0.662	6993 ± 118	0.929 ± 0.004	2.4 ± 0.04
DNA/GC	86.9 ± 0.6	21939 ± 322	0.915 ± 0.002	0.774 ± 0.01
NiONP–DNA/GC	88.2 ± 0.6	1069 ± 47	0.935 ± 0.005	15.8 ± 0.7

R_s: solution resistance; n: surface inhomogeneity parameter (which varies from zero to one, and is equal to one for completely smooth surface); R_{ct}: charge transfer resistance; K_{app}: apparent rate constant. $kapp = RT/n^2F^2R_{ct}CA$ for a redox system under diffusion control, where R_{ct} is charge transfer resistance; n is the number of electrons involved in the redox process ($n=1$); C is concentration of the redox probe; F is the Faraday number (96485 C eq^{-1}); R is gas constant 8.315 J $mole^{-1}$ K^{-1} and T is Kelvin temperature); and A is the surface area of the electrode.

An important question is: what is the origin of the decrease of R_{ct} of NiONPs after immobilization onto DNA/GCE compared to the bare GCE? Several assumptions can be made: (i) a complex (or precipitate) may form between NiONPs and $[Fe(CN)_6]^{3-/4-}$, which creates a mixed effect including diffusion-confined reaction of the redox probe, $[Fe(CN)_6]^{3-/4-}$, and surface-confined reaction of the *probably* formed $Ni_2[Fe(CN)_6]$ or $Ni_3[Fe(CN)_6]_2$ complex; (ii) an electrostatic interaction may occur between the probe and NiONPs immobilized on the electrode surface; and (iii) the different electron transfer properties of NiONP/GCE and NiONP–DNA/GCE may be attributed to their different surface morphologies. The first assumption was investigated by incubating both NiONP/GCE and NiONP–DNA/GCE electrodes in 0.5 mM $[Fe(CN)_6]^{3-/4-}$ for 30 min. Then, both electrodes were removed, washed thoroughly with water and subjected to CV measurements in a probe free PBS (pH 7). Both the recorded CVs contained only the background current, indicating that no reaction occurred between the immobilized NiONPs and $[Fe(CN)_6]^{3-/4-}$ probe under experimental condition.

Since, the immobilization mechanism of NiONPs on the DNA backbone is unknown, we were curious to see whether the decrease in R_{ct} observed on NiONP–DNA/GCE originated from the electrostatic attraction between $[Fe(CN)_6]^{3-/4-}$ and a positively charged complex that has been *probably* formed between NiO and DNA molecules. For this purpose, EIS experiments were performed in the presence of FcMeOH as the neutral redox system.

3.3.2. EIS study in the presence of FcMeOH

Since FcMeOH is a neutral redox probe, no electrostatic interaction occurs between the positively charged electrode surface and this molecule, and any changes in the R_{ct} can be attributed to the blocking effect of the immobilized layer(s) that hinder the surface. Fig. 3 shows the EIS Nyquist plots of the bare GCE (a), NiONP/GCE (b), DNA/GCE (c) and NiONP–DNA/GCE (d) in 0.10 M KCl solution containing 0.2 mM FcMeOH, at applied potential of 0.17 V (vs. Ag/AgCl). The kinetic parameters were obtained by fitting to the appropriate equivalent circuit (models ((A) and (B), the inset in Fig. 3) and the results are reported in Table 1B. Note that model (B) (one-CPE model without Warburg element) was applied whenever Warburg impedance was not observed. The estimates of R_{ct} obtained by fitting the data were found to be 1065,

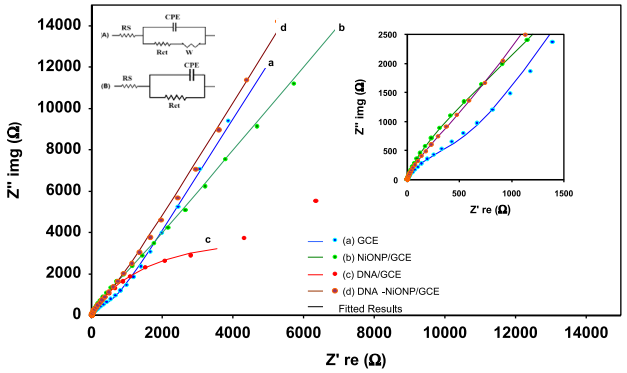

Fig. 3. The Nyquist plots obtained on GCE (a), NiONP/GCE (b), DNA/GCE (c), and NiONP–DNA/GCE (d) in 0.1 M KCl solution containing 0.2 mM FcMeOH at an applied potential of 0.17 V and a frequency range of $0.01–1\times10^4$ Hz. Symbols show the experimental data and symbols-trend lines shows the fitted data based on circuit models shown in inset top left: (A) for a, b and c; and (B) for c. Inset top right shows the EIS Nyquist plots at high frequency range.

Table 1B
Electrochemical parameters extracted from EIS data (Fig. 3) obtained on different modified electrodes in 0.1 M KCl containing 0.2 mM (FcMeOH).

Electrode	R_s (Ω)	R_{ct} (Ω)	n	K_{app}(cm s^{-1}) × 10^3
GC	1.796 ± 0.020	1069 ± 48	0.865 ± 0.003	39.8 ± 1.8
NiONP/GC	2.028 ± 0.007	2913 ± 98	0.914 ± 0.001	14.5 ± 0.5
DNA/GC	6.077 ± 0.063	8553 ± 372	0.836 ± 0.003	4.9 ± 0.2
NiONP–DNA/GC	2.369 ± 0.019	2171 ± 197	0.894 ± 0.003	19.5 ± 1.8

2913, 8553 and 2171 Ω for bare GCE, NiONP/GCE, DNA/GCE and NiONP–DNA/GCE, respectively. These observations support that was previously achieved from EIS experiments in the presence of $[Fe(CN)_6]^{3-/4-}$. Thus, the assumption for "the formation of a positive complex between NiONPs and DNA backbone" is not confirmed. Overall, no conclusive conclusion can be made and no mechanism can be offered for these apparent results, but it could be suggested that the facilitated electron transfer process at the NiONP–DNA/GCE is attributed to the higher fraction of sharp corners and edges present in the triangular NiONPs immobilized on the DNA-coated GCE compared to the spherical NiONPs immobilized on the bare GCE. Hence, DNA molecules played an important role in fabrication of the proposed sensor, not only in supplying more sites for immobilization of NiONPs, but also it acted as template for the construction of triangular nanoparticles with improved electron transfer properties.

3.4. Electrocatalytic activity of NiONP/GCE and NiONP–DNA/GCE toward glucose oxidation

The enzymatic detection systems usually suffer from chemical and thermal instabilities originated from intrinsic nature of enzymes, which limits their analytical applications (Siqueira Jr. et al., 2010). Recently, transition metal oxides (such as NiO, CuO and TiO_2) have been used in development of enzymeless glucose sensors (Toghill and Compton, 2010). Due to the fact that NiONP–DNA nanocomposite offers a larger NiONP surface coverage and more facile electron-transfer kinetics than the primitive NiONP film, the present modified electrode (NiONP–DNA/GCE) is expected to offer more efficient electrocatalytic activity compared to the NiONP/GCE. So, the electrocatalytic activity of the NiONP–DNA/GCE was investigated by measuring the catalytic current for the oxidation of glucose in alkaline media.

3.4.1. Cyclic voltammetry measurements

Fig. 4A shows CVs of NiONP/GCE (a and b) and NiONP–DNA/GCE (c and d) in 0.5 M NaOH solution in the absence (a and c) and presence (b and d) of 3 mM glucose recorded at a scan rate of 20 mV s^{-1}. For both modified electrodes, a clear increase in the anodic current and a decrease in the cathodic current were observed in the presence of glucose, which is expected for an electrocatalytic process. However, NiONP–DNA/GCE shows a remarkably higher voltammetric response towards glucose compared to NiONP/GCE. Under the same conditions, no redox response to glucose was observed at bare GCE (see inset of

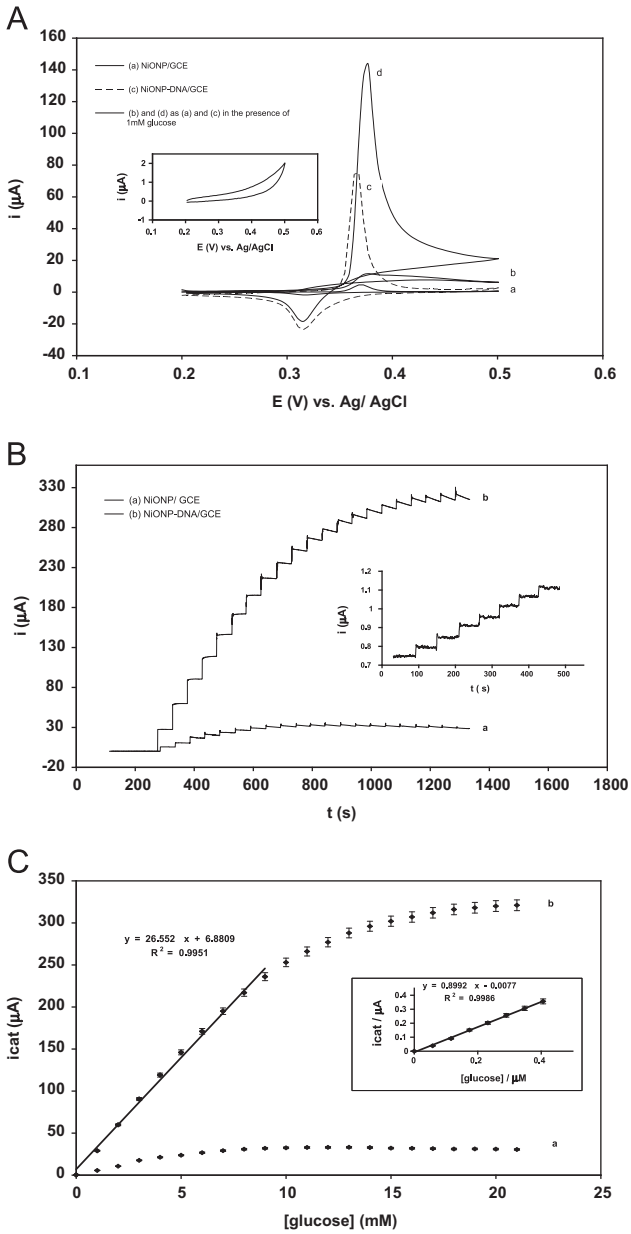

Fig. 4. (A) CVs of NiONP/GCE obtained in a 0.5 M NaOH solution at a scan rate of 20 mV s^{-1} in the absence (a) and presence of 3 mM glucose, (c) and (d) as (a) and (b) for NiONP–DNA/GCE. Inset: CV at the bare GCE obtained under the same conditions in the presence of glucose. (B) Amperometric responses of the rotating electrodes (rotation speed = 1500 rpm) of NiONP/GCE (a) and NiONP–DNA/GCE (b) to the successive additions of 1 mM glucose into 0.5 M NaOH solution at E 0.44 V. Inset: amperometric response of the rotating NiONP–DNA/GCE to successive additions of 0.058 μM glucose under the same conditions. (C) Calibration plots of the catalytic currents of NiONP/GCE (a) and NiONP–DNA/GCE (b) vs. glucose concentration. Inset: calibration plots of the catalytic currents of NiONP–DNA/GCE obtained due to the successive addition of 0.058 μM glucose.

Fig. 4A). The following catalytic scheme describes the reaction sequence in the oxidation of glucose by NiONPs (Niu et al., 2013):

$$Ni(OH)_2 + OH^- \rightarrow NiO(OH) + e^- + H_2O \quad (2)$$

$$NiO(OH) + glucose \rightarrow Ni(OH)_2 + glucolactone \quad (3)$$

It is important to note that the effective surface coverage, Γ, for NiONPs deposited on the DNA/GCE surface is 39.2 nmol cm^{-2}, which is ~6-fold greater than the value of Γ for NiONPs deposited on the bare GCE surface (Γ=6.2 nmol cm^{-2}). On the other hand, CVs at NiONP–DNA/GCE showed a catalytic current of 1.32 mA cm^{-2} for the oxidation of glucose, which is about 11-fold greater than that obtained at NiONP/GCE (0.121 mA cm^{-2}) at the same experimental conditions. This is particularly significant because it means that the enhancement of the catalytic ability of NiONP–DNA/GCE for the oxidation of glucose is not only due to the enhanced amount of NiONPs deposited on the DNA/GCE surface, but also due to facilitated electron transfer process at the NiONP–DNA/GCE interface. The above results provide additional evidence that electron transfer between NiONPs and the electrode surface is facilitated in the presence of the DNA layer.

3.4.2. Amperometric measurements

Since amperometry under stirred condition is more sensitive than cyclic voltammetry, this method was employed in order to estimate the lower detection limit of the sensor. Fig. 4B shows the steady-state current–time response of the rotating NiONP/GCE (curve a) and NiONP–DNA/GCE (curve b) to the successive addition of glucose in the range of 1–20 mM into 0.5 M NaOH solution at 0.44 V and rotation speed of 1500 rpm. The electrocatalytic anodic current sharply increased after each glucose addition and reached a steady-state behavior after about 10 s. As shown in Fig. 4B, NiONP–DNA/GCE exhibited remarkably higher amperometric responses to glucose at all concentrations compared to that of NiONP/GCE. Although both modified electrodes displayed relatively rapid response to glucose, the current response of NiONP/GCE leveled off to a saturation value after a few additions of glucose. The amperometric response of NiONP–DNA/GCE toward addition of 1 mM glucose into 0.5 M NaOH solution is linear up to 10 mM with a slope of 26.55 μA mM^{-1} (510.58 μA mM^{-1} cm^{-2}) and a correlation coefficient of 0.995 (Fig. 4C). In addition, based on calibration curve of NiONP–DNA/GCE at lower concentrations of glucose (Fig. 4C) during successive injection of 0.058 μM (inset of Fig. 4B), a sensitivity and a detection limit of 899.2 μAmM^{-1} (17.32 mA $mM^{-1}cm^{-2}$) and 17 nM were determined, respectively. This sensor represents prominent analytical performance for glucose detection in terms of the detection limit, linear concentration range and sensitivity, compared to the most sensitive Ni-based glucose sensors reported in the literature, as listed in Table 2A. These analytical data are especially impressive when considering that a small amount of NiONPs was immobilized on the electrode surface (~3.6 μg cm^{-2}). The enhanced analytical characteristics of the developed sensor can be attributed to the amount of NiONPs deposited on the DNA/GCE as well as facilitation of the electron transfer process at NiONP–DNA/GCE surface, which yield a significant enhancement in the electrocatalytic process.

The stability of NiONP–DNA/GCE toward the oxidation of glucose was investigated by amperometric technique. The electrode retained about 95% of its initial response to 0.1 mM glucose after 700 s (Fig. S4), indicating that the stability of NiONP–DNA/GCE toward the oxidation of glucose is satisfactory, and electrode surface fouling did not occur. The reproducibility of the sensor was estimated by determining 1.0 μM of glucose with five sensors which were prepared independently. The relative standard deviation was obtained to be 5.1%. Furthermore, the precision of the sensor was evaluated by 6 times repetitive measuring of 1.0 μM of glucose. The observed coefficient of variation was 4.2%.

One of the major problems in the electrochemical determination of glucose is the interference from the oxidation of common interfering species such as ascorbic acid (AA), uric acid (UA) and oxalic acid (OA). The effects of these interfering agents on the amperometric response of the modified electrode were evaluated in details (Figs. S5 and S6 and related discussions). The results interestingly exhibited that the amperometric response of the NiONP/GCE to negatively charged species such as AA and UA decreased as the amount of NiONPs on the surface was elevated (Fig. S5). So, the interference responses generated by these interfering agents can ideally be negligible in the presence of a high amount of NiONPs immobilized on the NiONP–DNA/GCE surface. In addition, the amperometric responses of NiONP–DNA/GCE to glucose in the presence of AA, UA and OA (0.1 mM, the normal concentration range in serum sample) is negligible (Fig. S6).

3.5. Glucose measurement in real sample

To evaluate the applicability of the developed nonenzymatic glucose sensor for real sample analysis, it was employed to determine the concentration of glucose in human blood serum samples. Five serum samples were prepared and diluted 3-fold with water before determination. The results obtained by the proposed glucose sensor are in good agreement with those measured with a commercial blood glucose monitoring system (Table 2B). So the developed sensor can be used for measuring the blood glucose with sufficient accuracy.

Table 2A
Comparison of performance of the glucose sensor fabricated in this work with some other nonenzymatic Ni-based glucose sensors.

Electrode	LOD (μM)	Sensitivity	Linear range (mM)
3D porous Ni networks (Niu et al., 2013)	0.07	2900 **μA/mM cm²**	0.0005–4
PtNi–ERGO/GCE (Gao et al., 2011)	10	20.42 **μA/mM cm²**	Up to 35
Ti/TiO_2 nanotube array Ni (Wang et al., 2010)	4	200 **μA/mM cm²**	0.1–1.7
Dendritic Cu – Ni/TiO_2 film (Tong et al., 2010)	0.35	661.5 **μA/mM cm²**	0.001–0.5
$Ni(OH)_2$ nanoparticle (Hutton et al., 2011)	0.4	330 **μA/mM cm²**	
NA/NiONF–rGO (Zhang et al., 2012)	0.77	1100 **μA/mM cm²**	0.002–0.60
Nano NiO–CPE (Mu et al., 2011)	0.16	43.9 nA/μM	0.001–0.11
Ni–MWNT (Sun et al., 2012)	0.89	67.2 **μA/mM cm²**	Up to 17.5
Nanostructured α-$Ni(OH)_2$ (Martins et al., 2011)	2.5	446 **μA/mM cm²**	0.01–0.75
Ni nanoparticles/MWCNT (Nie et al., 2011)	0.5	1438 **μA/mM cm²**	0.001–1
Ni CFP electrode (Liu et al., 2009)	1	3.30 μA/mM	0.02–2.5
Nanoscale $Ni(OH)_2$ (Safavi et al., 2009)	6	202 **μA/mM cm²**	0.5–23
NiONP–DNA (this study)	0.017	17292.69 **μA/mM cm²**	Up to 9

ERGO: electrochemical reduced graphene oxide; NA/NiONF–rGO: Nafion NiO nanofibers graphene oxide; CPE: carbon past electrode; and MWNT: multi-walled carbon nanotubes.

Table 2B
Determination of glucose in blood serum samples using NiONP–DNA/GCE.

Blood serum sample	Glucose concentration (mM) this sensor	Glucose concentration (mM) standard method	RSD (%, $n=3$)
1	5.00 ± 0.08	4.94	1.6
2	3.72 ± 0.04	3.71	1.1
3	5.74 ± 0.11	5.50	1.9
4	4.41 ± 0.08	4.40	1.8
5	4.40 ± 0.10	4.49	2.3

4. Conclusions

In summary, the electrodeposition method was used for the synthesis of NiONPs onto the bare GCE and DNA/GCE surfaces. The AFM measurements revealed the formation of triangular NiONPs deposited on the DNA/GCE surface, while the electrodeposition of NiONPs on the bare GCE surface leads to the formation of spherical NPs. The EIS investigations indicated that compared to the NiONP/GCE, the electron-transfer kinetics facilitated at the NiONP–DNA/GCE in the presence of different external redox probes ($[Fe(CN)_6]^{3-/4-}$ and FcMeOH), which can be attributed to the higher fraction of sharp corners and edges present in the triangular NiONPs compared to the spherical NPs. The electrocatalytic activities of NiONP/GCE and NiONP–DNA/GCE modified electrodes toward glucose oxidation were investigated. The electrochemical measurements revealed an 11-fold enhancement in the electrocatalytic activity of NiONP–DNA/GCE compared to that of NiONP/GCE, which can be ascribed to the ability of NiO–DNA nanocomposite to provide a larger NiONP surface coverage and more facile electron-transfer kinetics than the primitive NiONP film. The effect of most common interfering species in biological fluids such as AA, UA and OA on sensor response was negligible and finally, the proposed sensor was successfully applied to the determination of glucose in serum samples. This method of assembling triangular NiONPs on the DNA template may be expanded to other nanoparticles and is expected to have promising implications in the design of electrochemical sensors or biosensors.

Acknowledgments

The financial supports of Irananian Initiative Nanotechnology, Research Office of University of Kurdistan, and University of Isfahan are acknowledged.

Appendix. Supporting information

Supplementary data associated with this article can be found in the online version at http://dx.doi.org/10.1016/j.bios.2014.01.010.

References

An, H., Jin, B., 2012. Biotechnol. Adv. 30, 1721–1732.
Elyasi, M., Khalilzadeh, M., Karimi, H., 2013. Food Chem. 141, 4311–4317.
Gao, H., Xiao, F., Ching, C.B., Duan, H., 2011. ACS Appl. Mater. Interfaces 3, 3049–3057.
Giovanelli, D., Lawrence, N.S., Jiang, L., Jones, T.G.J., Compton, R.G., 2003. Sens. Actuators B 88, 320–328.
Hutton, L A., Vidotti, M., Patel, A.N., Newton, M.E., Unwin, P.R., Macpherson, J. V., 2011, J. Phys. Chem. C 115, 1658–1649.
Jiang, Q., Jiang, L., Hou, H., Qi, J., Wang, S., Sun, G., 2010. J. Phys. Chem. C 114, 19714–19722.
Karimi-Maleh, H., Biparva, P., Mehdi Hatami, M., 2013. Biosens. Bioelectron. 48, 270–275.
Khairy, M., El-Safty, S.A., Ismael, M., Kawarada, H., 2012. Appl. Catal. B 127, 1–10.
Kumar, A., Pattarkine, M., Bhadhade, M., Mandale, A.B., Ganesh, K.N., Datar, S.S., Dharmadhikari, C.V., Sastry, M., 2001. Adv. Mater. 13, 341–344.
Lakowicz, J.R., Gryczynski, I., Gryczynski, Z., Nowaczyk, K., Murphy, C.J., 2000. Anal. Biochem. 280, 128–136.
Lin, X., Jiang, X., Lu, L., 2005. Biosens. Bioelectron. 20, 1709–1717.
Liu, Y., Teng, H., Hou, H., You, T., 2009. Biosens. Bioelectron. 24, 3329–3334.
Martins, P.R., Aparecida Rocha, M., Angnes, L., Eisi Toma, H., Araki, K., 2011. Electroanalysis 23, 2541–2548.
Mu, Y., Jia, D., He, Y., Miao, Y., Wu, H.-L., 2011. Biosens. Bioelectron. 26, 2948–2952.
Narayanan, R., El-Sayed, M.A., 2004a. J. Am. Chem. Soc. 126, 7194–7195.
Narayanan, R., El-Sayed, M.A., 2004b. J. Phys. Chem. B 108, 5726–5733.
Nie, H., Yao, Z., Zhou, X., Yang, Z., Huang, S., 2011. Biosens. Bioelectron. 30, 28–34.
Niu, X., Lan, M., Zhao, H., Chen, C., 2013. Anal. Chem. 85, 3561–3569.
Noorbakhash, A., Salimi, A., 2011. Electrochim. Acta 56, 6097–6105.
Ojani, R., Raoof, J.-B., Zamani, S., 2012. Bioelectrochemistry 85, 44–49.
Peck, M.A., Langell, M.A., 2012. Chem. Mater. 24, 4483–4490.
Saadati, S., Salimi, A., Hallaj, R., Rostami, A., 2012. Anal. Chim. Acta 753, 32–41.
Safavi, A., Maleki, N., Farjami, E., 2009. Biosens. Bioelectron. 24, 1655–1660.
Salimi, A., Roushani, M., Soltanian, S., Hallaj, R., 2007a. Anal. Chem. 79, 7431–7438.
Salimi, A., Sharifi, E., Noorbakhsh, A., Soltanian, S., 2007b. Biosens. Bioelectron. 22, 3146–3153.
Sharifi, E., Salimi, A., Shams, E., 2013. Biosens. Bioelectron. 45, 260–266.
Siqueira , J.R., Caseli, L., Crespilho, F.N., Zucolotto, V., Oliveira , O.N., 2010. Biosens. Bioelectron. 25, 1254–1263.
Sun, A., Zheng, J., Sheng, Q., 2012. Electrochim. Acta 65, 64–69.
Sun, Y., Xia, Y., 2002. Science 298, 2176–2179.
Thimsen, E., Martinson, A.B.F., Elam, J.W., Pellin, M.J., 2012. J. Phys. Chem. C 116, 16830–16840.
Toghill, K.E., Compton, R.G., 2010. Int. J. Electrochem. Sci. 5, 1246–1301.
Tong, S., Xu, Y., Zhang, Z., Song, W., 2010. J. Phys. Chem. C 114, 20925–20931.
Wang, C., Yin, L., Zhang, L., Gao, R., 2010. J. Phys. Chem. C 114, 4408–4413.
Welch, C.M., Compton, R.G., 2006. Anal. Bioanal. Chem. 384, 601–619.
Wu, M.-S., Chang, H.-W., 2013. J. Phys. Chem. C 117, 2590–2599.
Xu, R., Wang, D., Zhang, J., Li, Y., 2006. Chem. Asian J. 1, 888–893.
Yin, Z., Wu, J., Yang, Z., 2011. Biosens. Bioelectron. 26, 1970–1974.
Zhang, Y., Wang, Y., Jia, J., Wang, J., 2012. Sens. Actuators B 171–172, 580–587.
Zhang, C., Park, Su-M., 1998. J. Electrochem. Soc. 136, 3333–3342.